Multi-carrier Directional Modulation Symbol Synthesis Using Time-Modulated Phased Arrays

Multi-carrier Directional Modulation Symbol Synthesis Using Time-Modulated Phased Arrays

Gaojian Huang, *Student Member, IEEE,* Yuan Ding, *Member, IEEE,* Shan Ouyang

***Abstract*—In this letter we present a new approach of using time modulated phased arrays (TMPAs) to synthesize multi-carrier directional modulation (DM) symbols for physical-layer security. In particular, the modulated waveform synthesis is achieved with the careful design of the switching time sequences, instead of in digital baseband, thus, reducing the peak-to-average power ratio (PAPR) of signals going through the radio frequency (RF) chain, and only a single RF chain is required here. The operation principle and synthesis approach are elaborated and demonstrated. In addition, the efficacy of the proposed DM approach is validated via the bit error rate (BER) metric.**

***Index Terms*—Beamforming gain, bit error rate (BER), directional modulation (DM), multi-carrier, peak-to-average power ratio (PAPR), time-modulated phased array (TMPA)**

I. Introduction

Directional Modulation (DM), is a transmitter-end technology that is capable of projecting digitally modulated information signals into pre-specified spatial directions while simultaneously distorting the constellation formats of the same signals in all other directions [1], thus, providing physical-layer wireless security. DM technology has gained increasing attention in recent years in wireless community. In [2]–[4], DM structures, which rely on pattern-reconfigurable arrays, were introduced. Later, the digital baseband DM solutions were proposed in [1], [5], [6]. The 'synthesis-free' DM implementation architectures were described in [7]–[9]. It should be noted that most of the previous DM systems only operate for single carrier signal transmissions.

Time-modulated array (TMA) is also referred as switched antenna array wherein 'time', turning on or off antennas, is introduced to the array design [10]. In its original form, it utilizes radio frequency (RF) switches to activate or deactivate, namely On-Off, each individual antenna in the array. This extra design degree of freedom endows its array radiation patterns some unique features. For instance, the array radiation pattern with ultra-low sidelobes was synthesized utilizing this TMA approach in [11]. In [12], Harr wavelets was applied onto TMAs to suppress the undesired harmonics. The generation of harmonic beamforming patterns by way of accurately controlling and adjusting the 'On-Off' sequence in a TMA was studied in [13]. Specifically, an extra state '–1' was suggested in [14], [15]. Here '–1' represents a phase shift of π which provides an additional degree of freedom in controlling radiation patterns. In [16], the TMA beamforming was further investigated. One major issue regard to TMA is the low power efficiency due to switching off some antenna elements periodically in the time domain. This problem can be alleviated by using reconfigurable beamforming networks [17], [18], which dynamically re-route energy to active array element. Some other approaches have also been reported. For example, non-ideal bipolar squared periodic sequences [19], single-pole double-throw switches [20] and alternately switching between array elements [21] were employed to improve efficiency. In [22], the signal bandwidth limitation of TMA was discussed, suggesting that the time modulation frequency should be larger than the signal bandwidth to avoid the aliasing effect. The properties of the TMA have been found useful for a number of applications. In [23], it was shown that the TMA can be exploited to achieve space division multiple access through modulating the synthesized fundamental and harmonic components. In [24], the four-dimensional antenna array (4-D AA) was used to achieve DM functionality through exploiting the aliasing effect (overlapping of modulated signal spectrum). Recently, utilizing the TMA to construct orthogonal frequency-division multiplexing (OFDM) directional modulation (DM) transmitter for physical-layer secured wireless communications was introduced in [25]. In this system, the multi-carrier OFDM signals are synthesized in digital baseband and the DM functionality is achieved by controlling switches to generate multi-carrier orthogonal artificial interference. One issue raised from this structure is the high signal peak-to-average power ratio (PAPR) which significantly reduces the efficiency of power amplifier in the RF chain.

In this letter, different to the works in [24], [25], we propose to both synthesize multi-carrier waveforms and enable DM functionality using three-state switches in the TMA. Here only constant-envelope RF carrier is needed.

The letter is organized as follows. In Section II, the time-modulated phased array (TMPA) transmitter architecture and the associated system assumptions are described, followed by the elaboration of the multi-carrier DM symbol synthesis principle and efficiency analysis. In Section III, the effectiveness of this proposed approach is validated through the simulations of two typical examples and BER metrics. Finally, conclusions are drawn in Section IV.

II. TMPA and Multi-carrier DM Symbol Synthesis

A. TMPA transmitter

The proposed transmitter architecture of a TMPA with a single RF chain is illustrated by an example of a one-dimensional (1D) M-element linear array with uniform spacing $d = \lambda_0/2$, where λ_0 is the wavelength of the input RF carrier of frequency f_0, seen in Fig. 1. At the transmitter side, an input RF carrier is firstly amplified by a power amplifier, before being divided into M identical copies with a 1-to-M power splitter. Then each signal copy goes through a phase shifter (with phase delay ϕ_m) followed by a single-pole triple-throw (SP3T) RF switch, setting the associated antenna excitation as 'On', 'Off' and

Mr. G. Huang's work was supported by the National Natural Science Foundation of China under Grant no.61871425 and Innovation Project of GUET Graduate Education. Dr Y. Ding's work was supported by the EPSRC (UK) under Grant EP/P025129/1.

G. Huang and S. Ouyang are with the School of Information and Communications, Guilin University of Electronic Technology, Guilin 541004, China (e-mails: gaojianhuang@yahoo.com and hmoysh@guet.edu.cn); S. Ouyang is also with the State and Local Joint Engineering Research Center for Satellite Navigation and Location Service (Guilin University of Electronic Technology), Guilin, Guangxi, China.

Y. Ding is with the Institute of Sensors, Signals and Systems (ISSS), Heriot-Watt University, Edinburgh EH14 4AS, U.K (e-mail: yuan.ding@hw.ac.uk)

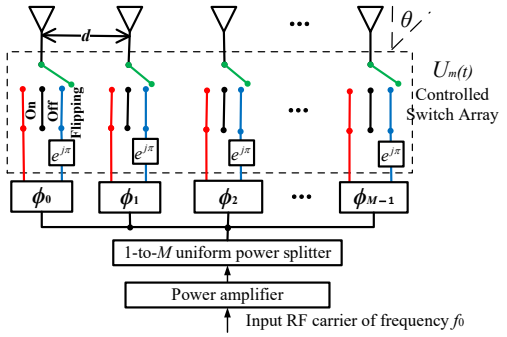

Fig. 1. TMPA transmitter with a single RF chain.

'Flipping', represented as '1', '0' and '–1', respectively. It is noted that the switches may require high-power handling capability. This demand can be relieved when the number of arrays is massive, i.e., large M. Here each active antenna element pattern is assumed to be isotropic and identical.

The far-field pattern of the TMPA in free space can be expressed as

$$F(\theta)=e^{j2\pi f_0 t}\cdot\sum_{m=0}^{M-1}\left(U_m(t)\cdot e^{jm\pi\sin\theta}\cdot e^{-j\phi_m}\right), \tag{1}$$

where θ is the spatial direction with the array boresight set as the angle reference, $\theta\in[-\pi/2,\pi/2]$. ϕ_m denotes the phase delay in the m^{th} antenna branch. $U_m(t)$ represents the periodic sequence function in time domain of the m^{th} SP3T RF switch. For better illustrating $U_m(t)$, three scenarios are depicted in Fig. 2. $U_m(t)$ in one period T_p can be expressed as

$$U_m(t)=\begin{cases}1 & t_m^{s_1}\le t\le t_m^{e_1}\ when\ t_m^{e_1}>t_m^{s_1},\ or\\ & 0\le t\le t_m^{e_1}\ and\ t_m^{s_1}\le t\le T_p\ when\ t_m^{e_1}<t_m^{s_1}\\ -1 & t_m^{s_2}\le t\le t_m^{e_2}\ when\ t_m^{e_2}>t_m^{s_2},\ or\\ & 0\le t\le t_m^{e_2}\ and\ t_m^{s_2}\le t\le T_p\ when\ t_m^{e_2}<t_m^{s_2}\\ 0 & otherwise\end{cases}. \tag{2}$$

It is noted that the $(t_m^{s_1}, t_m^{e_1})$ and $(t_m^{s_2}, t_m^{e_2})$ denote the switch (On, Off) time instants for the positive and negative cycles respectively, as seen in Fig. 2, and we define

$$\begin{cases}\Delta t_m^{(1)}=t_m^{e_1}-t_m^{s_1}\ when\ t_m^{e_1}>t_m^{s_1},\ or\\ \qquad\Delta t_m^{(1)}=T_p+t_m^{e_1}-t_m^{s_1}\ when\ t_m^{e_1}<t_m^{s_1}\\ \Delta t_m^{(2)}=t_m^{e_2}-t_m^{s_2}\ when\ t_m^{e_2}>t_m^{s_2},\ or\\ \qquad\Delta t_m^{(2)}=T_p+t_m^{e_2}-t_m^{s_2}\ when\ t_m^{e_2}<t_m^{s_2}\\ t_m^{s_2}=t_m^{s_1}+\Delta t_m^{(1)}+\delta\ when\ t_m^{e_1}>t_m^{s_1},\ or\\ \qquad t_m^{s_2}=t_m^{s_1}+\Delta t_m^{(1)}+\delta-T_p\ when\ t_m^{e_1}<t_m^{s_1},\ \delta\in[0,T_p)\end{cases}. \tag{3}$$

The periodic function $U_m(t)$ can be expanded into Fourier series as

$$U_m(t)=\sum_{q=-\infty}^{\infty}e^{j2\pi qf_p t}\cdot\left(\frac{\sin(\pi qf_p\Delta t_m^{(1)})}{q\pi}\cdot e^{-j\pi qf_p\left(2t_m^{s_1}+\Delta t_m^{(1)}\right)}-\frac{\sin(\pi qf_p\Delta t_m^{(2)})}{q\pi}\cdot e^{-j\pi qf_p\left(2t_m^{s_2}+\Delta t_m^{(2)}\right)}\right), \tag{4}$$

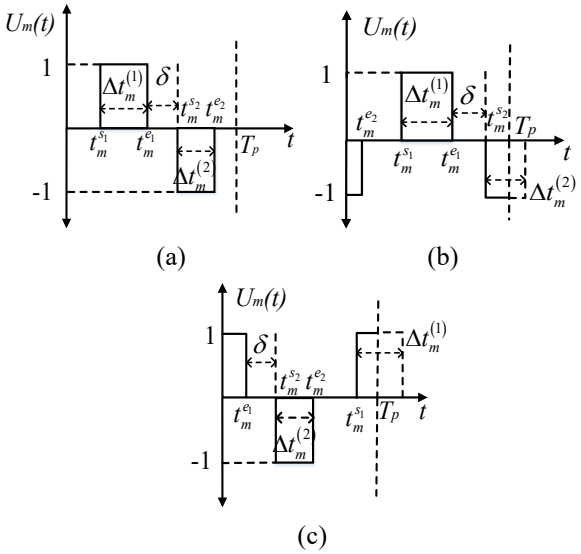

Fig. 2. Three cases of the switch function $U_m(t)$ in time domain.

where the time modulation frequency $f_p = 1/T_p$. Defining

$$\begin{cases}\tau_m^{s_1}=t_m^{s_1}/T_p,\ \tau_m^{s_2}=t_m^{s_2}/T_p,\ \rho=\delta/T_p\\ \tau_m^{(1)}=\Delta t_m^{(1)}/T_p,\ \tau_m^{(2)}=\Delta t_m^{(2)}/T_p\end{cases}, \tag{5}$$

and substituting (4) and (5) into (1), we get

$$F(\theta)=\sum_{q=-\infty}^{\infty}\left[e^{j2\pi(f_0+qf_p)t}\sum_{m=0}^{M-1}\left(\frac{\sin(q\pi\tau_m^{(1)})}{q\pi}-\frac{\sin(q\pi\tau_m^{(2)})}{q\pi}\cdot e^{-j\pi q\left(\tau_m^{(1)}+\tau_m^{(2)}+2\rho\right)}\right)\cdot e^{j\pi\left(m\sin\theta-\frac{\phi_m}{\pi}-q\left(2\tau_m^{s_1}+\tau_m^{(1)}\right)\right)}\right]. \tag{6}$$

B. Proposed multi-carrier DM symbol synthesis

When the TMPA being considered to synthesize multi-carrier symbols, T_p is set as the symbol period, and f_p can be seen as the frequency spacing between each two consecutive subcarriers. It is assumed that a legitimate user (LU) is located along the direction θ_L. ϕ_m in (6), similar to those in conventional phased arrays, is designed as $m\pi\sin\theta_0$. Thus, for the subcarrier at f_0+qf_p, the signals detected by the LU can be obtained from (6) and is expressed as

$$F_q(\theta_L)=\sum_{m=0}^{M-1}\left(\tau_m^{(1)}\,\mathrm{sinc}(q\tau_m^{(1)})-\tau_m^{(2)}\,\mathrm{sinc}(q\tau_m^{(2)})\cdot e^{-j\pi q\left(\tau_m^{(1)}+\tau_m^{(2)}+2\rho\right)}\right)\cdot e^{j\pi\left(m(\sin\theta_L-\sin\theta_0)-q\left(2\tau_m^{s_1}+\tau_m^{(1)}\right)\right)}, \tag{7}$$

where $\mathrm{sinc}(x)=\sin(\pi x)/(\pi x)$, and ρ has been defined in (5). From (7), for each subcarrier q, $F_q(\theta_L)$ needs to be synthesized for all possible constellation points in In-phase and Quadrature (IQ) space independently. For instance, when independent data are required to be binary phase shift keying (BPSK) modulated at subcarriers of f_0+f_p and f_0+2f_p, the following set of equations in (8) needs to have solutions. Here we assume $\tau_{mx}^{(1)}$, $\tau_{mx}^{(2)}$ and $\tau_{mx}^{s_1}$ are the set values/solutions of the variables $\tau_m^{(1)}$, $\tau_m^{(2)}$ and $\tau_m^{s_1}$, respectively, where x denotes index of produced constellation combination and $x = 1, 2, 3, 4$.

$$\begin{cases} F_1(\theta_L)_{(\tau_{m1}^{s_1},\tau_{m1}^{(1)},\tau_{m1}^{(2)},\rho,\theta_0,M)} = -F_1(\theta_L)_{(\tau_{m2}^{s_1},\tau_{m2}^{(1)},\tau_{m2}^{(2)},\rho,\theta_0,M)} \\ F_1(\theta_L)_{(\tau_{m1}^{s_1},\tau_{m1}^{(1)},\tau_{m1}^{(2)},\rho,\theta_0,M)} = F_1(\theta_L)_{(\tau_{m3}^{s_1},\tau_{m3}^{(1)},\tau_{m3}^{(2)},\rho,\theta_0,M)} \\ F_1(\theta_L)_{(\tau_{m2}^{s_1},\tau_{m2}^{(1)},\tau_{m2}^{(2)},\rho,\theta_0,M)} = F_1(\theta_L)_{(\tau_{m4}^{s_1},\tau_{m4}^{(1)},\tau_{m4}^{(2)},\rho,\theta_0,M)} \\ F_2(\theta_L)_{(\tau_{m1}^{s_1},\tau_{m1}^{(1)},\tau_{m1}^{(2)},\rho,\theta_0,M)} = -F_2(\theta_L)_{(\tau_{m3}^{s_1},\tau_{m3}^{(1)},\tau_{m3}^{(2)},\rho,\theta_0,M)} \\ F_2(\theta_L)_{(\tau_{m2}^{s_1},\tau_{m2}^{(1)},\tau_{m2}^{(2)},\rho,\theta_0,M)} = -F_2(\theta_L)_{(\tau_{m4}^{s_1},\tau_{m4}^{(1)},\tau_{m4}^{(2)},\rho,\theta_0,M)} \end{cases} \quad (8)$$

The solution sets from (8) are able to create four possible constellation combinations $[F_1(\theta_L), F_2(\theta_L)]$, namely $(\boldsymbol{C}_1, \boldsymbol{C}_2)$, $(\boldsymbol{C}_1, -\boldsymbol{C}_2)$, $(-\boldsymbol{C}_1, \boldsymbol{C}_2)$, $(-\boldsymbol{C}_1, -\boldsymbol{C}_2)$, where $\boldsymbol{C}_1$ and $\boldsymbol{C}_2$ can be any complex numbers that make (8) solvable. It is noteworthy that the desired constellation diagrams, i.e. signal waveforms, are projected into the spatial direction θ_L while along all other directions they are distorted, thereby enabling the DM functionality [1]. No closed-form solutions for (8) is available. Thus, the optimization algorithms, e.g. Particle Swarm Optimization (PSO), are selected, which have been widely adopted in other TMA works [13], [26]. In (7), $F_q(\theta_L)$ has six variable parameters i.e., $\tau_m^{(1)}$, $\tau_m^{(2)}$, $\tau_m^{s_1}$, ρ, θ_0 and M, which provide sufficient degrees of freedom to find out solution sets.

C. TMPA efficiency

The efficiency η of the TMPA here can be split into two separate efficiencies,

$$\eta = \eta^{\mathrm{F}} \cdot \eta^{\mathrm{H}} \quad (9)$$

where η^{F} denotes the feeding network efficiency which is caused by SP3T RF switches in the feeding network when the switches are off, and η^{H} denotes the harmonic efficiency. Here, the harmonic efficiency η^{H} is defined as the output power of useful harmonics divided by that of all harmonics. Since each branch is independent in TMPA, η^{F} and η^{H} can be expressed as [20]

$$\eta^{\mathrm{F}} = \frac{1}{M} \cdot \sum_{m=0}^{M-1} \left(\tau_m^{(1)} + \tau_m^{(2)} \right) \quad (10)$$

and

$$\eta^{\mathrm{H}} = \sum_{q\in\Gamma} \sum_{m=0}^{M-1} \left| c_{qm} \right|^2 / \sum_{q=-\infty}^{\infty} \sum_{m=0}^{M-1} \left| c_{qm} \right|^2, \quad (11)$$

where

$$c_{qm} = \frac{1}{T_p} \int_0^{T_p} U_m(t) e^{-j2\pi q f_p t} dt \quad (12)$$

and 'Γ' is the set of useful harmonics. At the harmonic frequency $f_0 + qf_p$, the radiated power is $4\pi \sum_{m=0}^{M-1} \left| c_{qm} \right|^2$, see [19].

III. Multi-carrier DM Symbol Synthesis Examples and BER Metrics

In this section, we show two typical examples of DM symbol synthesis and compare the BER simulation metrics with other TMA DM schemes.

A. Multi-carrier DM BPSK symbol synthesis at frequencies $f_0 + f_p$ and $f_0 + 2f_p$

From (6), at frequencies $f_0 + f_p$ and $f_0 + 2f_p$, the array patterns can be expressed as

TABLE I The multi-carrier DM BPSK symbol synthesis at $f_0 + f_p$ and $f_0 + 2f_p$, $\theta_L = 30°$.

m	$\tau_m^{(1)}$	$\tau_m^{(2)}$	$\tau_m^{s_1}$	$\tau_m^{(1)}$	$\tau_m^{(2)}$	$\tau_m^{s_1}$	$\tau_m^{(1)}$	$\tau_m^{(2)}$	$\tau_m^{s_1}$	$\tau_m^{(1)}$	$\tau_m^{(2)}$	$\tau_m^{s_1}$
0	0.3	0.69	0.87	0.62	0.26	0.74	0.22	0.7	0.41	0.57	0.37	0.26
1	0.27	0.7	0.03	0.33	0.3	0.15	0.6	0.32	0.59	0.3	0.35	0.69
2	0.47	0.31	0.37	0.26	0.68	0.36	0.6	0.38	0.71	0.28	0.24	0.83
3	0.33	0.34	0.66	0.26	0.62	0.54	0.39	0.29	0.12	0.58	0.35	0.08
4	0.3	0.65	0.82	0.67	0.31	0.67	0.32	0.62	0.36	0.61	0.32	0.23
5	0.68	0.29	0.01	0.3	0.27	0.2	0.31	0.21	0.49	0.33	0.28	0.67
6	0.19	0.33	0.66	0.33	0.57	0.33	0.65	0.29	0.67	0.31	0.66	0.86
7	0.61	0.31	0.37	0.58	0.31	0.66	0.36	0.29	0.15	0.25	0.7	0.02
	$F_1(\theta_L) \doteq 3.6$ $F_2(\theta_L) \doteq 2$			$F_1(\theta_L) \doteq 3.6$ $F_2(\theta_L) \doteq -2$			$F_1(\theta_L) \doteq -3.6$ $F_2(\theta_L) \doteq 2$			$F_1(\theta_L) \doteq -3.6$ $F_2(\theta_L) \doteq -2$		
	$q = 1$ BPSK 1 $q = 2$ BPSK 1			$q = 1$ BPSK 1 $q = 2$ BPSK 0			$q = 1$ BPSK 0 $q = 2$ BPSK 1			$q = 1$ BPSK 0 $q = 2$ BPSK 0		

$$F_1(\theta) = \sum_{m=0}^{M-1} \left(\tau_m^{(1)} \operatorname{sinc}(\tau_m^{(1)}) - \tau_m^{(2)} \operatorname{sinc}(\tau_m^{(2)}) \cdot e^{-j\pi\left(\tau_m^{(1)} + \tau_m^{(2)} + 2\rho\right)} \right) \cdot e^{j\pi\left(m\left(\sin\theta - \sin\theta_0\right) - \left(2\tau_m^{s_1} + \tau_m^{(1)}\right)\right)} \quad (13)$$

and

$$F_2(\theta) = \sum_{m=0}^{M-1} \left(\tau_m^{(1)} \operatorname{sinc}(2\tau_m^{(1)}) - \tau_m^{(2)} \operatorname{sinc}(2\tau_m^{(2)}) \cdot e^{-2j\pi\left(\tau_m^{(1)} + \tau_m^{(2)} + 2\rho\right)} \right) \cdot e^{j\pi\left(m\left(\sin\theta - \sin\theta_0\right) - 2\left(2\tau_m^{s_1} + \tau_m^{(1)}\right)\right)}, \quad (14)$$

respectively. In this example, we aim to synthesize BPSK modulation at frequency $f_0 + f_p$ and $f_0 + 2f_p$, thus four constellation combinations are required by properly designing the $\tau_m^{(1)}$, $\tau_m^{(2)}$ and $\tau_m^{s_1}$. It is assumed that $\theta_L = 30°$, $\theta_0 = 0$, $\rho = 0$, and $M = 8$. One of solution sets, obtained by the PSO algorithm, are shown in TABLE I. The patterns at frequencies $f_0 + f_p$ and $f_0 + 2f_p$ are depicted in Fig. 3(a)–(d). It can be

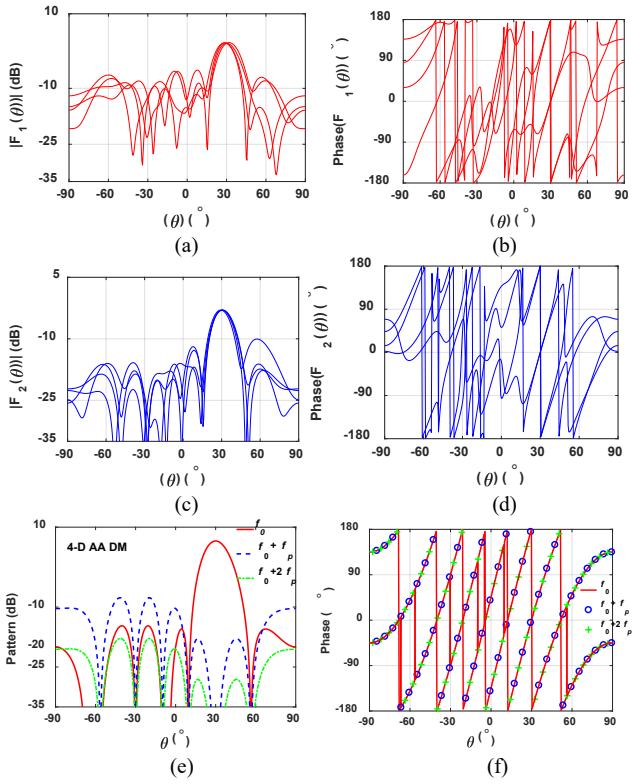

Fig. 3. The normalized far-filed patterns, (a), (c) magnitudes and (b), (d) phases; (a), (b) at frequency $f_0 + f_p$ and (c), (d) at frequency $f_0 + 2f_p$ in the example shown in TABLE I; (e) magnitudes and (f) phases in 4-D AA DM scheme [24]. θ_L is set to 30°.

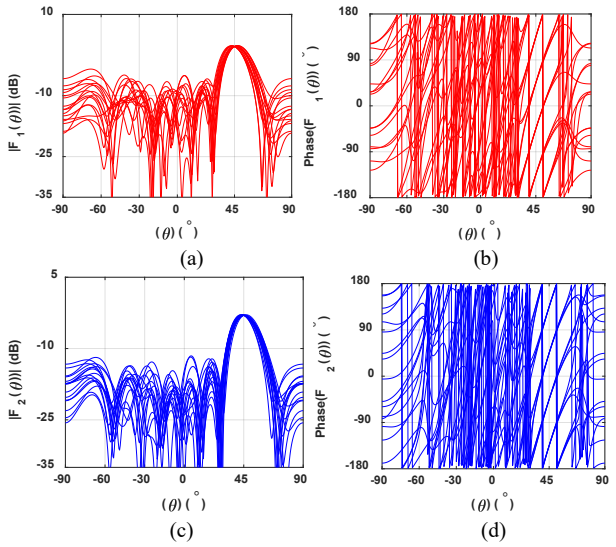

Fig. 4. The normalized far-filed patterns, (a), (c), magnitudes and (b), (d), phases. (a), (b) at frequency $f_0 + f_p$ and (c), (d) at the frequency $f_0 + 2f_p$. θ_L is set to 45°.

observed that the BPSK symbols are synthesized respectively at frequency $f_0 + f_p$ and $f_0 + 2f_p$ along the secure spatial direction θ_L, while in other directions, the patterns are distorted. In contrast, in the 4-D AA DM scheme [24], only the magnitude of harmonic frequency is suppressed along the desired direction, while the phases are well preserved in all spatial directions, indicating that the information can be intercepted by demodulating harmonic frequency signals in free space. Thus, to achieve DM functionality, in the 4-D AA DM scheme the signal bandwidth must be greater than f_p in order to create frequency aliasing effect. In the proposed TMPA DM scheme, when $\tau_m^{(1)}$, $\tau_m^{(2)}$, $\tau_m^{s_1}$, ρ, θ_0 and M are fixed, e.g. in Table I, η^F and η^H can be calculated. For example, when BPSK symbol '11' is synthesized, we get $\eta^F = 84.61\%$ and $\eta^H = 38.84\%$. It is noted that the values of η^F and η^H are different for different synthesized BPSK symbols since the chosen parameters $\tau_m^{(1)}$, $\tau_m^{(2)}$ and $\tau_m^{s_1}$ are not fixed. Intuitively, the harmonic efficiency η^H can be improved when more subcarriers are used for DM transmissions.

B. *Multi-carrier DM QPSK symbol synthesis at frequencies $f_0 + f_p$, $f_0 + 2f_p$*

In this example, two independent quadrature phase shift keying (QPSK) data streams at frequencies $f_0 + f_p$ and $f_0 + 2f_p$ are transmitted simultaneously to the LU located at $\theta_L = 45°$. This requires to create sixteen constellation combinations, such as ($\boldsymbol{C}_1 e^{j\pi/4}$, $\boldsymbol{C}_2 e^{j\pi/4}$), ($\boldsymbol{C}_1 e^{j\pi/4}$, $\boldsymbol{C}_2 e^{-j\pi/4}$), ($\boldsymbol{C}_1 e^{j\pi/4}$, $\boldsymbol{C}_2 e^{3j\pi/4}$), ($\boldsymbol{C}_1 e^{j\pi/4}$, $\boldsymbol{C}_2 e^{-3j\pi/4}$). In Fig. 4, the patterns corresponding to one of solution sets at the two frequencies are depicted. Similarly, it can be observed that two independent QPSK modulated signals are formed at these two different frequencies, and beamforming gain and DM functionality are enabled. It is also worth pointing out that each pattern in Fig. 4 (a) and (c) is associated with only one transmitted symbol, and the more meaningful radiation energy along the sidelobe directions is the average of all possible patterns. In this sense, the synthesized sidelobe level (SLL) is always kept below –10 dB.

Based on the proposed multi-carrier DM symbol synthesis approach, some aspects are now emphasized,

- The DM symbols are synthesized via controlling RF switches rather than in digital baseband, resulting in a PAPR of 0 dB;
- The beamforming gains toward the LU can be controlled by setting the three parameters, i.e., $\tau_m^{(1)}$, $\tau_m^{(2)}$ and M. The transmit antenna number M here not only affects the beamforming gain but also determines the number of constellation combinations. When ρ and θ_0 are fixed, there are $3M$ variables, allowing us to synthesize $3M$ constellation combinations across multiple subcarriers;
- The solution sets for synthesizing constellation combinations are not unique, thus the power at each modulated subcarrier frequency can be adjusted by fully exploiting the degrees of freedom provided by $\tau_m^{(1)}$, $\tau_m^{(2)}$, $\tau_m^{s_1}$, ρ, θ_0 and M;
- The synthesis of higher order modulations may make the optimization process time consuming due to the number of possible constellation symbol combinations across all subcarriers is huge;
- The eavesdropper user (EU), as generally assumed in most reported wireless security literature, is configured to be the same as the LU, e.g. the same receiving frequency bands. When this is assumed, the proposed system is able to secure the transmission in all spatial directions rather than a narrow direction range around θ_L. When a stronger assumption is made, i.e. the EU has the knowledge of which frequency bands it should be tuned and which subcarrier order the signals are arranged, in the shown examples it becomes possible for this advanced eavesdropper to intercept information along $-\theta_L$. To address this issue, it will require non-symmetrical switching functions.

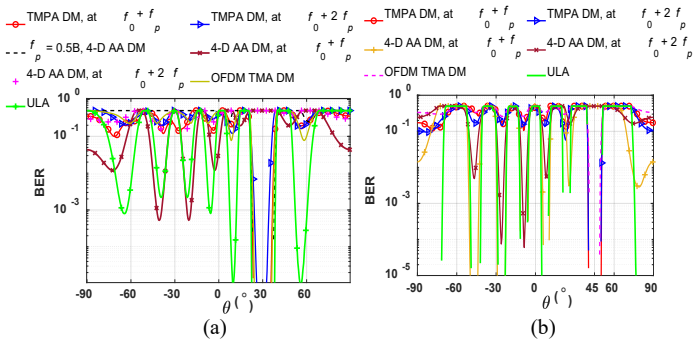

Fig. 5. Simulated BERs of various DM schemes, (a) BPSK, at SNR = 15 dB; (b) QPSK, at SNR = 30 dB.

C. *BER metrics*

In Fig. 5, BER performance of the proposed multi-carrier TMPA DM (the two aforementioned examples), the 4-D AA DM, the OFDM TMA DM and the conventional uniform linear array (ULA) schemes are respectively depicted at different signal-to-noise ratios (SNRs). It can be observed that, at frequencies $f_0 + f_p$ and $f_0 + 2f_p$ in the proposed DM scheme regardless of BPSK or QPSK symbol synthesis, the BER main beams are focused along the desired direction and the BER sidelobes are suppressed in other directions, suggesting the information can be secured along the pre-specified spatial direction. By contrast, in the 4-D AA DM scheme, information can be eavesdropped at each harmonic frequency in the undesired directions, see Fig. 5(b). For the ULA, obviously information transmission is not secured due to the high BER sidelobes. It is noted that the OFDM TMA DM can also secure wireless transmission, but at the cost of high PAPR.

IV. Conclusion

This letter presented a novel multi-carrier DM symbol synthesis approach by exploiting a single RF chain TMPAs. In the proposed approach, the multi-carrier DM symbols were synthesized in RF feeding networks via switches rather than in the digital baseband, resulting in the constant envelop RF carriers which enjoy low PAPR. The low PAPR would, in turn, allow power amplifiers operation in high-efficiency saturation region. This proposed technique therefore is

useful in secure multi-carrier wireless communication applications.

REFERENCES

[1] Y. Ding and V. F. Fusco, "A vector approach for the analysis and synthesis of directional modulation transmitters," *IEEE Trans. Antennas Propag.*, vol. 62, no. 1, pp. 361–370, Jan. 2014.

[2] A. Babakhani, D. Rutledge, and A. Hajimiri, "Near-field direct antenna modulation," *IEEE Microw. Mag.*, vol. 10, no. 1, pp. 36–46, Feb. 2009.

[3] M. P. Daly and J. T. Bernhard, "Directional modulation technique for phased arrays," *IEEE Trans. Antennas Propag.*, vol. 57, no. 9, pp. 2633–2640, Sep. 2009.

[4] M. P. Daly and J. T. Bernhard, "Beamsteering in pattern reconfigurable arrays using directional modulation," *IEEE Trans. Antennas Propag.*, vol. 58, no. 7, pp. 2259–2265, Jul. 2010.

[5] A. Kalantari, M. Soltanalian, S. Maleki, S. Chatzinotas, and B. Ottersten, "Directional modulation via symbol-level precoding: A way to enhance security," *IEEE J. Sel. Topics Signal Process.*, vol. 10, no. 8, pp. 1478–1493, Dec. 2016.

[6] J. Hu, F. Shu and J. Li, "Robust synthesis method for secure directional modulation with imperfect direction angle," *IEEE Commun. Lett.*, vol. 20, no. 6, pp. 1084–1087, Jun. 2016.

[7] N. Valliappan, A. Lozano, and R. W. Heath, "Antenna subset modulationfor secure millimeter-wave wireless communication," *IEEE Trans. Commun.*, vol. 61, pp. 3231–3245, Aug. 2013.

[8] Y. Ding and V. Fusco, "A synthesis-free directional modulation transmitter using retrodirective array," *IEEE J. Sel. Topics Signal Process.*, vol. 11, no. 2, pp. 428–441, Mar. 2017.

[9] Y. Ding, V. Fusco, and A. Chepala, "Circular directional modulation transmitter array," *IET Microw., Antennas Propag.*, vol. 11, no. 3, pp.1909–1917, Oct. 2017.

[10] W.-Q Wang, H. So, and A. Farina, "An overview on time/frequency modulated array processing," *IEEE J. Sel. Topics Signal Process.*, vol.11, no. 2, pp. 228–246, Mar. 2017.

[11] W. H. Kummer, A. T. Villeneuve, T. S. Fong, and F. G. Terrio, "Ultra low sidelobes from time-modulated arrays," *IEEE Trans. Antennas Propag*., vol. 11, no. 6, pp. 633–639, Nov. 1963.

[12] R. Maneiro-Catoira, J. Brégains, J. A. García-Naya and L. Castedo, "Time-modulated arrays with Haar wavelets," *IEEE Antennas Wireless Propag. Lett.*, vol. 19, no. 11, pp. 1862–1866, Nov. 2020.

[13] L. Poli, P. Rocca, G. Oliveri, and A. Massa, "Harmonic beamforming in time-modulated linear arrays," *IEEE Trans. Antennas Propag.*, vol.59, no. 7, pp. 2538–2545, Jul. 2011.

[14] G. Bogdan, Y. Yashchyshyn and M. Jarzynka, "Time-modulated antenna array with lossless switching network," *IEEE Antennas Wireless Propag. Lett.*, vol. 15, pp. 1827–1830, 2016.

[15] H. Li, Y. Chen, and S. Yang, "Harmonic beamforming in antenna array with time-modulated amplitude-phase weighting technique," *IEEE Trans. Antennas Propag*., vol. 67, no. 10, pp. 6461–6472, Oct. 2019.

[16] R. Maneiro-Catoira, J. Brégains, J. A. García-Naya, and L. Castedo, "Time-modulated array beamforming with periodic stair-step pulses," *Signal Process.*, vol. 166, 2020, Art. no. 107247.

[17] J. Chen et al., "Efficiency improvement of time modulated array with reconfigurable power divider/combiner," *IEEE Trans. Antennas Propag*., vol. 65, no. 8, pp. 4027–4037, Aug. 2017.

[18] Q. Chen, J. Zhang, W. Wu and D. Fang, "Enhanced single-sideband time-modulated phased array with lower sideband level and loss," *IEEE Trans. Antennas Propag*., vol. 68, no. 1, pp. 275–286, Jan. 2020.

[19] R. Maneiro-Catoira, J. Brégains, J. A. García-Naya and L. Castedo, "Time-modulated phased array controlled with nonideal bipolar squared periodic sequences," *IEEE Antennas Wireless Propag. Lett.*, vol. 18, no. 2, pp. 407–411, Feb. 2019.

[20] Q. Zhu, S. Yang, R. Yao and Z. Nie, "Gain improvement in time-modulated linear arrays using SPDT switches," *IEEE Antennas Wireless Propag. Lett.*, vol. 11, pp. 994–997, 2012.

[21] G. Bogdan, K. Godziszewski, Y. Yashchyshyn, C. H. Kim and S. -B. Hyun, "Time-modulated antenna array for real-time adaptation in wideband wireless systems—Part I: design and characterization," *IEEE Trans. Antennas Propag*., vol. 68, no. 10, pp. 6964–6972, Oct. 2020.

[22] R. Maneiro-Catoira, J. C. Brégains, J. A. García-Naya and L. Castedo, "On the feasibility of time-modulated arrays for digital linear modulations: a theoretical analysis," *IEEE Trans. Antennas Propag*., vol. 62, no. 12, pp. 6114–6122, Dec. 2014.

[23] C. He, X. L. Liang, B. Zhou, J. P. Geng, and R. H. Jin, "Space-division multiple access based on time-modulated array," *IEEE Antennas Wireless Propag. Lett.*, vol. 14, no. 1, pp. 610–613, 2015.

[24] Q. Zhu, S. Yang, R. Yao and Z. Nie, "Directional modulation based on 4-D antenna arrays," *IEEE Trans. Antennas Propag*., vol. 62, no. 2, pp. 621–628, Feb. 2014.

[25] Y. Ding, V. Fusco, J. Zhang, and W. Wang, "Time-modulated OFDM directional modulation transmitters," *IEEE Trans. Veh. Technol*., vol. 68, no. 8, pp. 8249–8253, Aug. 2019.

[26] L. Poli, P. Rocca, L. Manica and A. Massa, "Handling sideband radiations in time-modulated arrays through particle swarm optimization," *IEEE Trans. Antennas Propag.*, vol. 58, no. 4, pp. 1408–1411, April 2010.